Surface Engineering for Molecular Electronics

Qiu, Xinkai

DOI:
10.33612/diss.146270150

2

Mechanically and Electrically Robust Self-assembled Monolayers for Large-area Tunneling Junctions

The contents of this chapter have been published in *J. Phys. Chem. C* **2017**, 121, 14920-14928. We acknowledged Dr. Y. Zhang for the synthesis and EGaIn measurements, S. Soni for DFT calculation and Dr. T.L. Krijger for XPS measurements.

2

ABSTRACT

*This chapter examines the relationship between mechanical deformation and the electronic properties of self-assembled monolayers (SAMs) of the oligothiophene 4-([2,2':5',2":5",2"'-quarterthiophene]-5-yl)bytane-1-thiol (**T4C4**) in tunneling junctions using conductive probe atomic force microscopy (CP-AFM) and eutectic Ga-In (EGaIn). We compared shifts in conductivity, transition voltages of **T4C4** with increasing AFM tip force loads to alkanethiolates. While these shifts result from an increasing tilt angle from penetration of the SAM by the AFM tip for the latter, we ascribe them to distortions of the π system present in **T4C4**, which is more mechanically robust than alkanethiolates of comparable length; SAMs comprising **T4C4** shows about five times higher Young's modulus than alkanethiolates. Density functional theory calcualtions confirm that mechanical deformations shift the barrier height due to changes in the frontier orbitals caused by small rearrangements to the conformation of the quaterthiophene moiety. The mechanical robustness of **T4C4** manifests as an increased tolerance to high bias in large-area EGaIn junctions suggesting that electrostatic pressure plays a significant role in the shorting of molecular junctions at high bias.*

2.1. INTRODUCTION

Emerging challenges in information technology are driving research into new computer architectures and circuit designs[1] that require new materials and concepts in nanoelectronics. Molecular electronics, specifically tunneling junctions comprising discrete molecules, are well suited to address these challenges[2, 3] because they control charge-transport directly at the quantum level, however, it remains impractical to integrate single-molecule junctions[4, 5] into devices. Bottom-up junctions comprising self-assembled monolayers[6–8] (SAMs), on the other hand, can already be incorporated into wafer-scale fabrication processes[9] and diode logic circuits[10]. When molecules pack into a SAM, collective effects, such as the overlap of interacting electronic states and charges, give rise to new properties that affect tunneling charge-transport significantly as compared to single-molecule junctions.[11–14] In addition to electronic and electrostatic effects, SAMs exhibit mechanical properties derived from the interactions between individual molecules, which play a critical role in the tolerance of SAMs toward particular top-contact and, ultimately, technological applications. Small changes in the conformation of a molecule or ensemble of molecules (*e.g.,* in a SAM) between two electrodes can have dramatic effects on conductance by altering electronic states in the metal/molecule/metal junction.[12, 15] Large-area junctions are typically constructed using SAMs of molecules with anchoring groups such as thiols that drive self-assembly into ordered structures that impose fixed conformations. The effects of these conformations and their relationship to the bulk mechanical properties of the SAM can not be ignored, particularly for π-conjugated molecules, since intermolecular interactions affect charge transport via electrostatic effects and because both hopping and tunneling charge-transport are sensitive to electronic delocalization, which is maximized in coplanar conformations. Establishing a structure-function relationship between mechanical deformation and electrostatics in SAMs of π-conjugated molecules is, therefore, important fundamentally and for the potential for exploitation in molecular-scale devices that are sensitive to force/pressure/deformation (see also **Chapter 1.1** for a survey of large-area junctions).

Conductive probe atomic force microscopy (CP-AFM) is capable of characterizing the electrical properties of SAMs while varying the force load applied to a probe tip that doubles as a top-contact. Changes in the resistances of SAMs of alkanethiolates with applied force have been ascribed to changes in the tilt angle of the alkyl chains.[16–20] Transition voltage spectroscopy (TVS) indicates that the transition voltage V_{trans} shifts to a lower bias with increasing force (*i.e.,* as the tilt angle increases).[19, 20] This observation implies a decrease in barrier height of molecular junctions because V_{trans} is proportional to the energy offset between the Fermi level E_{f} and the highest-occupied molecular state.[21] If there are more subtle influences to the electrostatics of the junctions from bond distortions they are masked by the larger effect of the tilt angle increasing as the tip penertrates the SAM, which is stabilized only by relatively weak intermolecular dispersion forces. The mechanical properties of SAMs of π-conjugated molecules have not been similarly investigated. Thus, my collaborator Yanxi Zhang synthesized 4-([2,2':5',2":5",2"'-quarterthiophene]-5-yl)butane-1-thiol (**T4C4**), a molecule containing both a flexible butanethiol chain to facilitate the formation of a densely packed monolayer and a rigid quarterthiophene to impart mechanical stability through relatively strong π-π

interactions. The molecular structure and the geometry of a CP-AFM junction are shown in Fig. 2.1. We studied the mechanical electrical properties SAMs of **T4C4** using CP-AFM and density functional theory (DFT). They are quantitatively more robust than SAMs of alkanethiolates, but the electrostatics of the junction respond to small distortions of the π-system. This robustness translates into junctions that are capable of withstanding larger bias windows than alkanethiolates in large-area junctions using eutectic Ga-In (EGaIn) top-contacts (see also **Chapter 1.3.2** for the introduction of EGaIn electrode).[22]

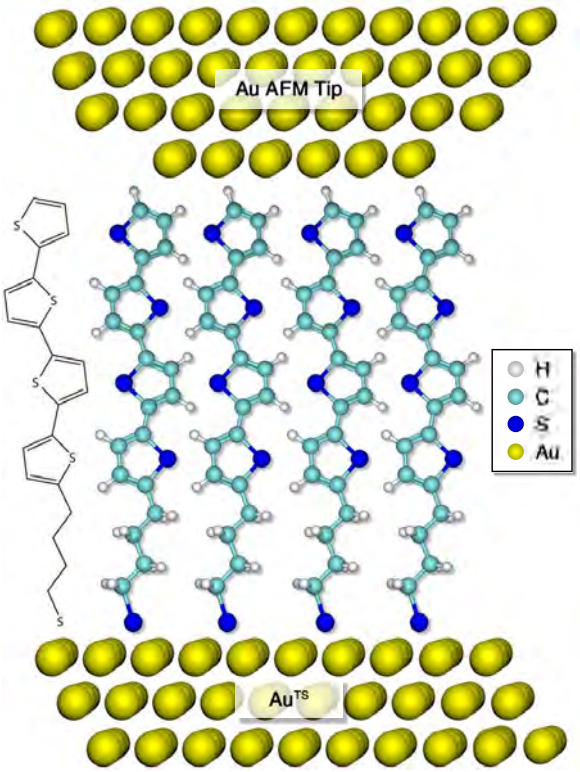

Figure 2.1 | Representative schematic of molecular junction comprising **T4C4** with a Au coated CP-AFM tip as top electrode and template-stripped Au as bottom electrode.

2.2. RESULTS AND DISCUSSION

We synthesized **T4C4**, a "σ-π" hybrid molecular structure containing both alkyl (σ) and thiophene (π) moieties according to the protocol described in literature.[23] We chose **T4C4** because it is known to form densely packed SAMs.[24–26] For comparison to previously reported mechanical studies, we used decanethiol (**C10**). We chose **C10** specifically because the properties of SAMs of **C10** have been studied extensively by CP-AFM.[16, 27, 28] We prepared both template-stripped gold (Au^{TS}) and silver (Ag^{TS}) ultrasmooth electrodes following template-stripping procedures in literature.[29] These

substrates are particularly well suited to large-area junctions[30] and are compatible with CP-AFM[12].

2.2.1. CP-AFM MEASUREMENTS

We formed metal-molecule-metal junctions by placing the gold coated CP-AFM tip (denoted Au^{AFM}) with spring constant of 0.35 N m^{-1} and radius of 30 nm in a stationary point contact with the SAM under a controlled tip force load, which translates into an applied pressure that depends on the radius of the tip; CP-AFM tips are larger than ordinary Si_3N_4 tips due to the additional metallic layers. We refer to the molecular junctions as Au^{TS}/SAM//Au^{AFM}, where "/" and "//" denote a covalent interface and a van der Waals contact, respectively. We measured the I/V characteristics of Au^{TS}/**C10**//Au^{AFM} and Au^{TS}/**T4C4**//Au^{AFM} junctions at low applied forces, which we define as 25 nN or less. Characteristic data are shown in Fig. 2.2 for **C10** and **T4C4**. (The I/V curves for **C10** at and above 25 nN shorted when bias was applied and are, therefore, omitted from the figure.) The I/V characteristics of **C10** were sufficiently similar to published data to validate our measurement technique.[16–20] The I/V curves of **T4C4** did not change at low forces (Fig. 2.2a), passing approximately 10 nA at 1 V. The I/V curves of **C10**, however, varied by about a factor of 2, passing approximately 200 nA at 1 V with a force of 10 nN and 100 nA at 1.4 nN (Fig. 2.2b). We were only able to measure **T4C4** to ±1 V without saturating the current amplifier, where we were able to measure **C10** to ±1.5 V using the low-gain amplifier because the absolute current in the intermediate-bias regime (*i.e.*, where the I/V dependence becomes exponential) increases more slowly for **C10** than for **T4C4**.

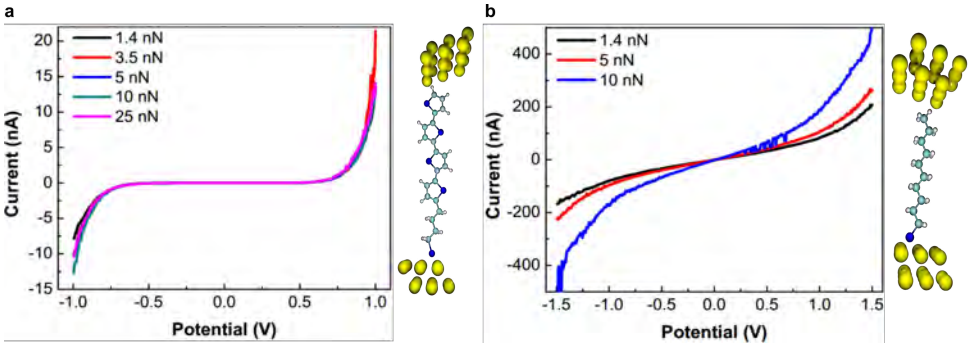

Figure 2.2 | Characterization of the charge transport properties of SAMs of **T4C4** and **C10** on Au^{TS} under varied force loads. **a**, I/V plots of **T4C4** measured under different force loads: 1.4 nN (black), 3.5 nN (red), 5 nN (blue), 10 nN (dark cyan) and 25 nN (pink). **b**, I/V plots of **C10** measured under different force loads: 1.4 nN (black), 5 nN (red) and 10 nN (blue). Both SAMs were measured on Au^{TS} substrates by CP-AFM.

The I/V curves of **T4C4** are sigmoidal, passing nearly invariant, low current in the linear, low-bias regime (below 0.5 V) and increasing dramatically in the exponential, intermediate-bias regime, which is consistent for π-conjugated (or σ-π) "molecular wire" molecules.[31] The I/V curves of **C10** are sigmoidal, but increase throughout the low-bias regime, which is consistent for alkanethiols.[16, 32] The evolution of the I/V curves with increasing force load can be caused by any combination of three factors: i) the

molecular tilt increases; ii) molecules in the SAM are deformed; and iii) the contact area increases. As mentioned above, the response of **C10** is attributed mainly to the tilt angle, but **T4C4** showed no change at forces up to 30 nN as can be seen in Fig. 2.3. (Note that the dependence of pressure on force load is nonlinear due to the dependence of contact area on force, thus the values across the top X-axis are only meant to show the range of pressures experienced by the SAM. See Methods section and Table 2.5 for the translation.) The semilog scale plot compresses the data somewhat, but there is still a clear, increasing trend for **C10** that is absent for **T4C4** even up to 30 nN (*i.e.*, three times the force load). At high force (30-150 nN) the conductivity of **T4C4** begins to increase, but **C10** either shorts or saturates the current amplifier (both manifest as hitting the compliance limit) above 10 nN (Fig. 2.4). Thus, we measured SAMs of dodecanethiol (**C12**) in Ag^{TS}/**C12**//Au^{AFM} and Ag^{TS}/**C12**//EGaIn junctions in order to compare the effects at high forces. We switched to Ag^{TS} substrates for **C12** to facilitate comparisons to literature as described below.[33–35] We also measured Ag^{TS}/**T4C4**//Au^{AFM} and Ag^{TS}/**T4C4**//EGaIn junctions for comparison. The increase in current of Ag^{TS}/**C12**//Au^{AFM} as a function of force load is even more dramatic than Au^{TS}/**C10**//Au^{AFM} and Ag^{TS}/**C10**//Au^{AFM}, spanning 3 orders of magnitude up to 150 nN (Figs. 2.5 and 2.6).

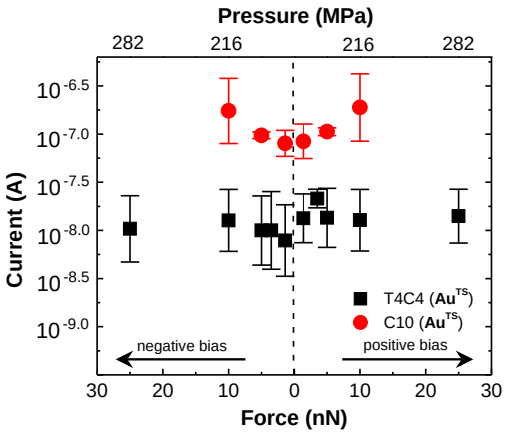

Figure 2.3 | Current measured on **T4C4** (black square) and **C10** (red circle) at 1 V versus force load on Au^{TS} substrates. Each data point is the peak of Gaussian fit to a histogram of I at the value of V. The error bars are standard deviations from Gaussian fit. The values listed on the top X-axis are the pressures calculated explicitly for the corresponding values of force on the bottom X-axis.

2.2.2. MECHANICAL PROPERTIES

In addition to I/V measurements via CP-AFM, we measured the mechanical properties of SAMs of **T4C4** and **C10** on Au^{AFM} using PeakForce quantitative nanomechanical mapping (PFQNM) AFM. Fig. 2.7 shows the deformation as a function of force load up to 7 nN. To enable a comparison between these data and CP-AFM data, we estimated the pressure applied to the SAM by considering the force load and the radius of the tip (see Methods section and Table 2.5). At force loads below 3 nN, the magnitudes and slopes are similar,

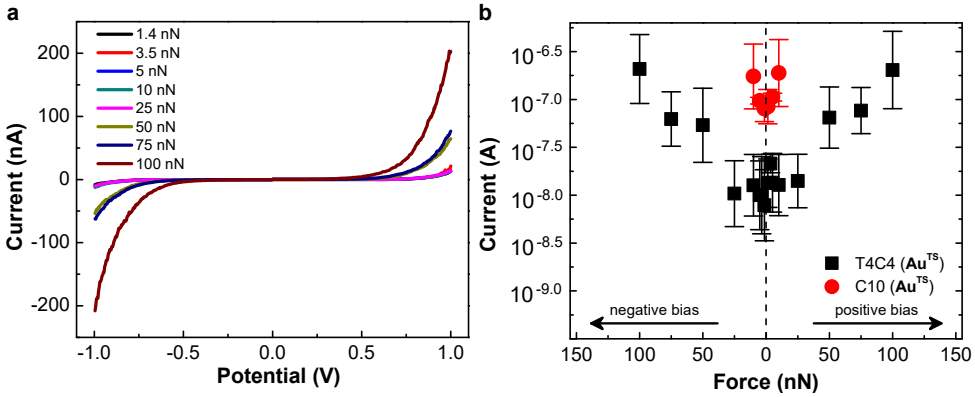

Figure 2.4 | Characterization of the charge transport properties of SAMs of **T4C4** and **C*n*** on Au^{TS} under varied force loads. **a**, *I*/*V* plots of **T4C4** on Au^{TS} (Au^{TS}/**T4C4**//CP-AFM) with different forces from 1.4 nN to 100 nN. **b**, Semi-log plot of current of **T4C4** (black square) and **C10** (red circle) on Au^{TS} at 1.0 V or -1.0 V versus force.

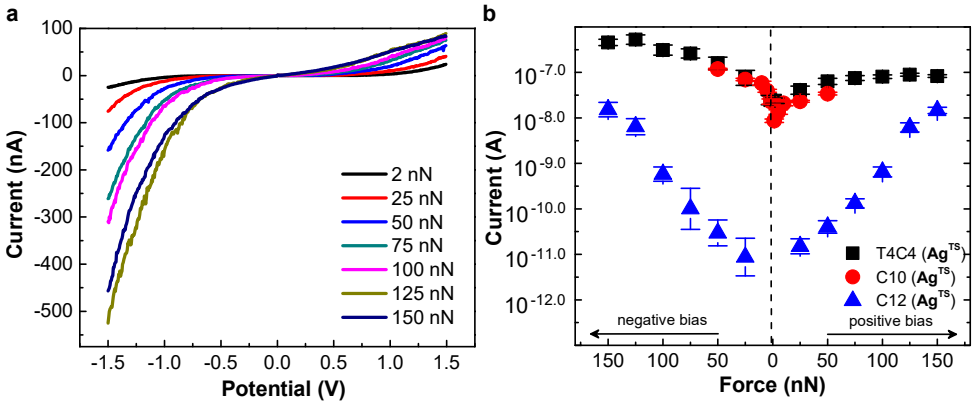

Figure 2.5 | Characterization of the charge transport properties of SAMs of **T4C4** and **C*n*** on Ag^{TS} under varied force loads. **a**, *I*/*V* plots of **T4C4** on Ag^{TS} (Ag^{TS}/**T4C4**//Au^{AFM}) with the force varied from 2 nN to 150 nN. **b**, Plots of log|*I*| of **T4C4** (black square), **C10** (red circle) and **C12** (blue triangle) on Ag^{TS} at 1.5 V or -1.5 V versus force.

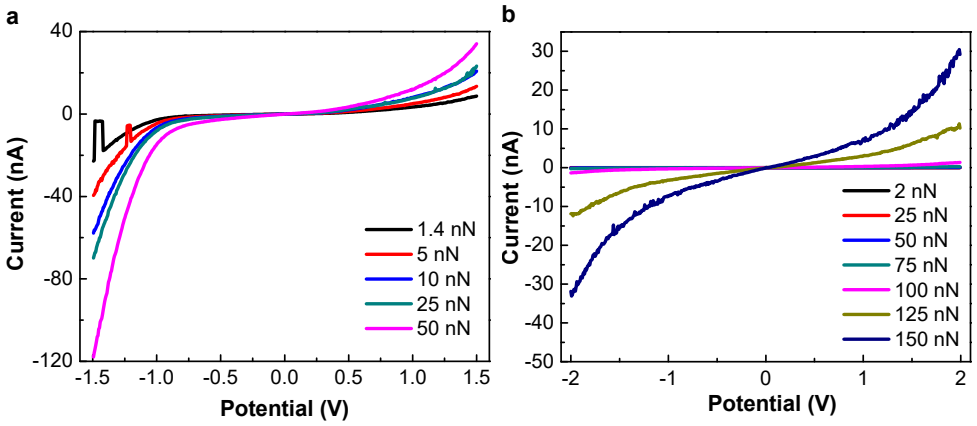

Figure 2.6 | Characterization of the charge transport properties of SAMs of **C*n*** on Ag^{TS} under varied force loads. **a**, I/V plots of **C10** on Ag^{TS} (Ag^{TS}/**C10**//Au^{AFM}) with the force varied from 1.4 nN to 50 nN. **b**, I/V plots of **C12** on Ag^{TS} (Ag^{TS}/**C12**//CP-AFM) with the force varied from 2 nN to 150 nN.

but above 3 nN the displacement of **T4C4** begins to level off at approximately 0.8 nm while **C10** continues to increase. We hypothesize that the inflection point in the **T4C4** curve is caused by compression/deformation of the butyl tail, which deforms at lower force load than the quarterthiophene unit (but similar to **C10**). Fig. 2.7b shows the Derjaguin-Muller-Toporov (DMT) Young's modulus, which is a measure of stiffness in the elastic region by taking adhesive contact into account in comparison to the conventional Hertzian model which assumes frictionless surfaces, over the same range of force load.[36, 37] (There are no error bars because the Young's modulus was calculated from the average deformation of each force load using the DMT model.) The difference is unambiguous; the modulus of **T4C4** is five times higher than **C10**, indicating that SAMs of **T4C4** are considerably stiffer than SAMs of **C10**. Our measured values for **C10** are also in good agreement with the moduli for SAMs of alkanethiolates reported previously; 280 MPa for octanethiol (**C8**) and 860 MPa for **C12**.[38] From the electrical and mechanical measurements, we concluded that SAMs of **T4C4** are more mechanically robust than **C10**, which translates into more stable conductance across a wider range of force loads; however, conductance alone does not provide much insight into the electrostatics of the junctions or address the question of why the I/V characteristics of **T4C4** are stable despite deforming considerably at low force loads.

2.2.3. TRANSITION VOLTAGE SPECTROSCOPY

Transition voltage spectroscopy (TVS) is a useful tool to gain insights into the electrostatics of molecular junctions by providing an indirect measure of ϕ, the offset between E_f and the frontier orbital that participates most strongly in tunneling transport (the highest occupied state for both **C10** and **T4C4**, *i.e.*, hole transport). The transition voltage V_{trans} corresponds to the transition from ohmic, low-bias conduction to exponential/hyperlinear conduction at intermediate bias, which can be estimated by replotting

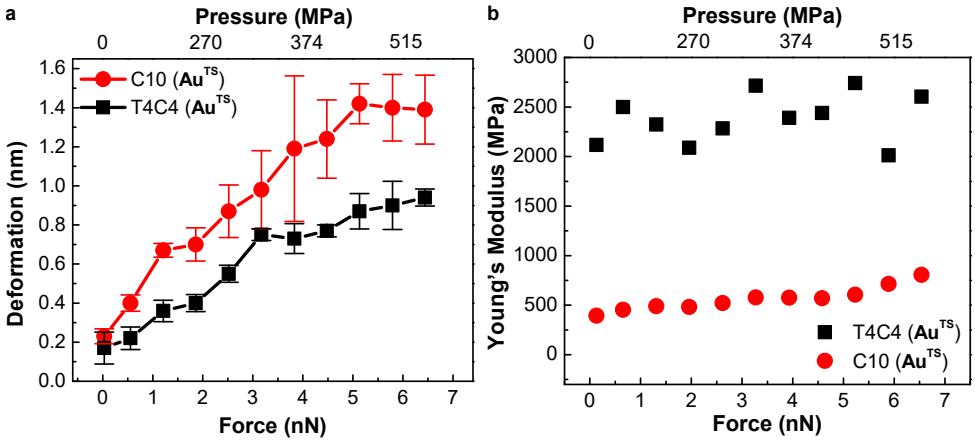

Figure 2.7 | Characterization of the mechanical properties of the SAMs of **T4C4** and **C10**. **a**, Deformation of SAMs of **T4C4** (black square) and **C10** (red circle) measured under different force loads on Au^{TS}. The error bars are standard deviations. **b**, Young's modulus of SAMs of **T4C4** (black square) and **C10** (red circle) measured under different force loads on Au^{TS}. The values listed on the top X-axis are the pressures calculated explicitly for the corresponding values of force on the bottom X-axis.

the I/V curves and looking for minimums.[21] The value of V_{trans} is proportional to the height of the tunneling barrier imposed by ϕ. Shifts in V_{trans}, therefore, reveal changes to ϕ, which is a function of the electrostatics (*i.e.*, level-alignment) near E_f. These shifts can occur independently of changes in conductance, either because they are below the threshold for detection or are offset by other changes, for example, the barrier width, which is related to the distance between the electrodes and, therefore, decreases as the SAM deforms. To compute V_{trans}, we plotted $ln(IV^{-2})$ vs V^{-1} using the peaks of Gaussian fits of histograms of I for each value of V at different force loads (200 traces for **T4C4** and 30 for **C10**) and recorded the center of the dips in the plots. These data are plotted in Fig. 2.8 and summarized in Table 2.1. At force load above 75 nN, the dips were not very pronounced, but they were well-resolved at all other forces, revealing clear differences between **T4C4** and **C10**.

The trend for **C10** shown in Fig. 2.8 and Table 2.1 is in excellent agreement with literature values; V_{trans}^{+} (V_{trans} at positive bias) decreases from a maximum of 1.20 to 0.95 V, a change of approximately 20%. Table 2.2 compares literature values of V_{trans}^{+} for **C8**, **C10** and **C12** at low force load to our value for **C10**; these values, which are typically 1.10 to 1.40 V for alkanethiols, are also in excellent agreement.[28, 39] Because V_{trans} is proportional to ϕ and E_f is invariant (*i.e.*, the value for Au^{TS}), V_{trans} is almost always smaller for π-conjugated molecules than for alkanethiols by virtue of the fact that the HOMO tends to lie closer to E_f.[40, 41] Indeed, V_{trans}^{+} for **T4C4** is about one-third the value of **C10**. Moreover, it decreases from 0.4 to 0.13 V, a change of approximately 70% over a range of 1.4 nN to 100 nN. From 1.4 nN to 10 nN, the range over which **C10** could be measured, **T4C4** only changes by approximately 5%, compared to 20% for **C10**. Thus, the changes in conductance in both SAMs correspond to a lowering of the barrier height, but it requires about 1 order of magnitude higher force load to induce a change in **T4C4** as

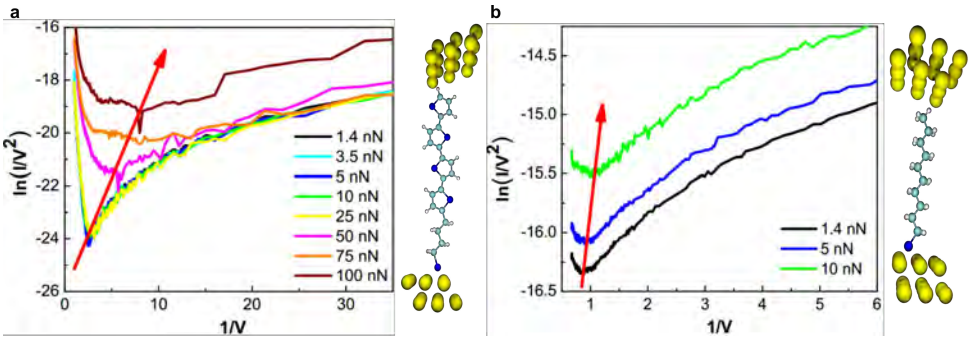

Figure 2.8 | Transition voltage spectroscopy of Au^{TS}/SAM//Au^{AFM} junctions versus force loads from the peaks of Gaussian fits obtained by CP-AFM at each force load. **a**, **T4C4**, 200 traces at each force load. **b**, **C10**, 30 traces at each force load. The equivalent pressures for each force are shown in Table 1.

compared to **C10**. Given the substantial differences in chemical structure and mechanical properties, it is unlikely that the cause of the shifts in V_{trans} are the same for **T4C4** as they are for **C10** (*i.e.*, increased tilt angle).

Table 2.1 | Measured values of V_{trans}^{+} at different force loads.

Pressure (MPa)	Force (nN)	V_{trans}^{+} (V)	
		T4C4	**C10**
163.12	1.4	0.4	1.20
177.35	3.5	0.4	-
186.94	5.0	0.4	1.10
215.93	10	0.38	0.95
282.28	25	0.34	-
352.43	50	0.18	-
396.49	75	0.14	-
426.72	100	0.13	-

2.2.4. DFT CALCULATIONS

For insights into the electrostatics of SAMs of **T4C4** under deformation, my colleague Saurabh Soni constructed model junctions and computed their properties using DFT. We include the results and discussion of the computation in the chapter for the integrity of whole story and as a support for the conclusion. The model junctions consist of single molecules spanning two clusters of Au atoms; these are not meant as direct simulations of Au^{TS}/SAM//Au junctions, rather, they are computationally accessible models from which we can compute trends to compare to experimental data. First, we optimized the geometry of the molecule in the gas-phase using B3LYP/6-311G*. Given the co-planar geometry of the quarterthiophene moiety and the tendency for alkanes to adopt a trans-extended conformation in SAMs, this geometry is a reasonable approximation for **T4C4** in a SAM. Second, we attached a cluster of Au at a hollow site via the thiol anchor on one

Table 2.2 | Comparison of $V_{trans}{}^{+}$ of alkanethiols on Au substrate at low force loads to literature values.

	$V_{trans}{}^{+}$ (V)		
	C8	**C10**	**C12**
this work	-	1.20	-
ref [28]	1.28	1.27	1.20
ref [39]	1.21	-	1.33
ref [42]	1.31	1.25	1.29
ref [43]	1.26	-	-

end and positioned an identical cluster above the terminal thiophene ring/methyl group at the other end. (The Au-S and Au-thiophene distances do have a small effect on the computed electrostatics, but they are kept constant across all calculations such that the effect is constant.)

Finally, we computed point energies using B3LYP/LANL2DZ for the molecule before and after attaching the metal electrodes to compare the orbital energies and isoplots of the molecule in gas phase and in the model junctions, respectively. To model the deformation of the SAM, we distorted the **T4C4** molecules in the model junctions systematically either by hand or by using displacements predicted from frequency calculations. The figure of merit of these calculations is the offset between the metal Fermi level and the highest-occupied π-state (HOPS) of **T4C4** (E_f-E_{HOPS}), which is a direct approximation of ϕ and, therefore, will vary accordingly with V_{trans}. Because these are Gaussian (*i.e.*, discrete, aperiodic) calculations the 'HOMO' corresponds to E_f, thus we locate the HOPS by comparing the model junction to the gas-phase calculation.

We estimated E_f-E_{HOPS} of SAMs of **T4C4** on Au^{TS} and Ag^{TS} experimentally from ultraviolet photoelectron spectroscopy (UPS) data according to ref [41] (Table 2.3). To relate the DFT calculations to experimental data, we computed E_f-E_{HOPS} using the value of E_f from UPS and the value of E_{HOPS} from DFT of the minimized geometry of **T4C4** in a model Au/**T4C4**/Au junction. This method produced excellent agreement for E_f-E_{HOPS} between UPS and DFT.

Table 2.3 | Energy levels determined by UPS.

	HOPS (eV)		E_f-E_{HOPS} (eV)	
	center	**onset**	**center**	**onset**
T4C4 on Au	−5.42	−4.88	1.23	0.68
T4C4 on Ag	−5.25	−4.71	1.31	0.77

Fig. 2.9 shows E_f-E_{HOPS} of model junction as a function of in-plane bending. Unsurprisingly, there is hardly any effect on **C10**, however, the response of **T4C4** is non-linear, increasing at first and then rapidly decreasing. The initial increase is due to the decrease in orbital overlap in the π-system, which lowers the energy of the HOPS (the total energy still increases). It is not clear why E_f-E_{HOPS} then decreases, but since we did not observe any increase in V_{trans} experimentally, we conclude that in-plane bending (a relatively high-energy deformation, particularly in a SAM) does not play a large role in the mechanical

deformation of SAMs of **T4C4**; we cannot exclude its contribution to **C10**, however.

In-plane bending is a relatively high-energy process. Deformations in which atoms are allowed to displace along all vibrational vectors are generally lower-energy processes, but are more difficult to rationalize because it translates a compressive force (from the AFM tip) into motion in all directions within a SAM. Nonetheless, molecules of **T4C4** stretched and compressed along these vectors show a linear response of E_f-E_{HOPS} as a function of relative displacement as is shown in Fig. 2.10. This response (as we go from 'stretched' to 'compressed' forms) also correctly predicts the direction of change in V_{trans}. Given the high Young's modulus and relatively small tip displacement, we hypothesize that the shifts in V_{trans} for Au^{TS}/**T4C4**//Au junctions are, therefore, the result of compressing molecules of **T4C4** along displacement vectors corresponding to vibrational modes that are allowed by the constraints of the SAM. This is a very different mechanism from that of **C10** and provides a coherent explanation for the change in conductance that occurs at high force loads. Other bending and twisting modes yielded either no change or an increase in V_{trans}.

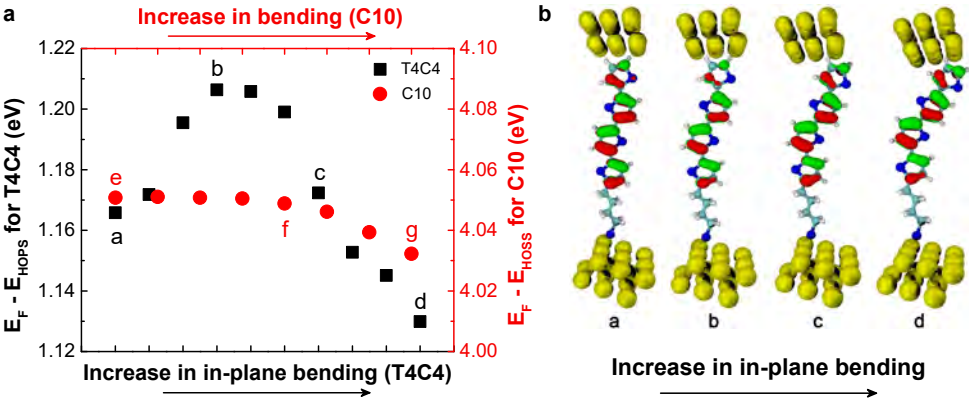

Figure 2.9 | DFT calculation of the frontier states of **T4C4** and **C10** over in-plane bending. **a**, Shift in the energy of E_f-E_{HOPS} of Au^{TS}/SAM//Au model junctions with the increased in-plane bending of the **T4C4** molecules (black squares), and E_f-E_{HOSS} with the increased bending of **C10** alkanethiol molecules (red dots), relative to their equilibrium geometries. The labeled data points (a, b, c and d) correspond to the energies of the **T4C4** geometries showed in the schematic (panel **b**). The first points a and e correspond to optimized geometries of **T4C4** and **C10** molecules, respectively. The geometries corresponding to the data points e, f, and g and further details are given in the Supporting Information. The E_f of Au electrodes was set to −4.20 eV for these plots from the UPS measurements.

2.2.5. STABILITY OF LARGE-AREA JUNCTIONS

The studies enumerated above probe areas on the order of tens of nm^2 to give insight into the bulk mechanical properties of a SAM (*e.g.,* stiffness,) however, the electrical properties that SAMs exhibit in large-area junctions include the influence of defects (*e.g.,* local disorder) driven by inhomogeneities in the substrate, chemical impurities and grain boundaries.[29, 44–46] Shorter alkanethiols exhibit more resilience to defects because they are more liquid-like;[47] however, when a voltage is applied to a large-area

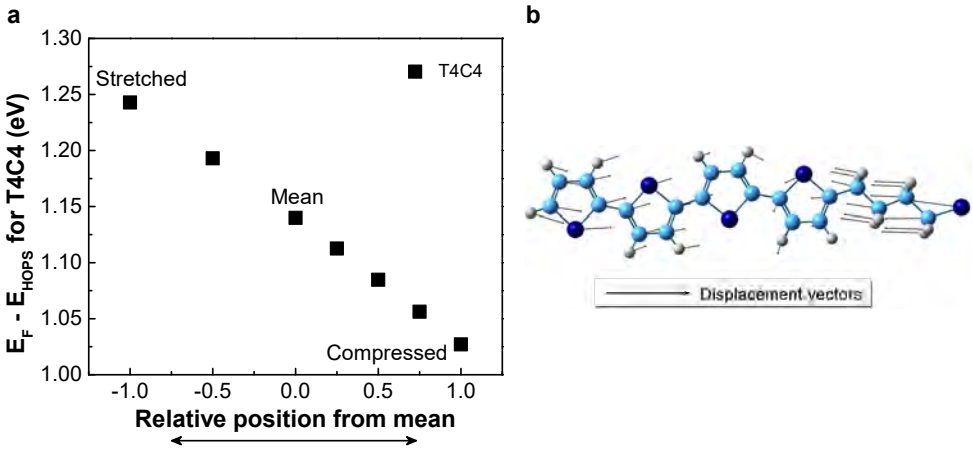

Figure 2.10 | DFT calculation of the frontier states of **T4C4** under stretching or compression. **a**, Shift in the energy of E_f-E_{HOPS} of Au^{TS}/**T4C4**//Au model junctions as a function of the displacement of atoms along vibrational vectors from frequency calculations. The points on X-axis span from −1 (fully stretched geometry) to +1 (fully compressed geometry), where 0 corresponds to the equilibrium geometry. **b**, The arrows represent the displacement vectors of individual atoms as they vibrate. The E_f of Au electrodes was set to −4.20 eV for these plots from the UPS measurements.

junction, a substantial electrostatic pressure develops that can deform and induce the reorganization[48] in which case the stiffness of longer alkyl chains is advantageous. We hypothesize that there is, therefore, a relationship between the mechanical stability of a SAM and its breakdown voltage; SAMs that can withstand higher electrostatic pressures should form large-area tunneling junctions that resist shorting at high bias. There is no consensus on the mechanism of failure of large-area junctions at high bias, which could be i) entirely a function of the ability of a SAM to resist penetration by the top-contact[49–51], ii) the migration of metal atoms from the bottom-contact[52, 53], *e.g.,* the formation of filaments of Au, iii) electrochemical instability[54] or iv) some combination of the three. A clear correlation between breakdown voltage and the mechanical robustness of **T4C4** would imply that mechanism i) is dominant because the electrochemical window of **T4C4** is much smaller than that of an alkanethiol. Extending the potential window in which a SAM can operate in a large-area junction is particularly relevant to molecule diodes[55] such as SAMs incorporating ferrocenyl,[56, 57] bipyridyl[58, 59], pyrimidyl[14], fullerene[60] moieties because the degree of rectification tends to scale with bias and they function under bias in integrated circuits.[10]

To investigate the influence of mechanical stability on breakdown voltages in large-area molecular junctions, we formed Ag^{TS}/SAM//EGaIn junctions[22] of **T4C4**, **C12**, tetradecanethiol (**C14**) and hexadecanethiol (**C16**). As mentioned above, we chose Ag^{TS} because it is the most commonly reported substrate for EGaIn top-contacts. We swept junctions of each SAM through increasing bias windows and recorded the frequency of shorts, defined by the sudden increase in current to the compliance limit of the instrument. Fig. 2.11a shows representative I/V plots (on a linear scale) revealing a clear trend of increasing breakdown potential: **T4C4** > **C16** > **C14** ≈ **C12** > **C10**. Fig. 2.11b shows the

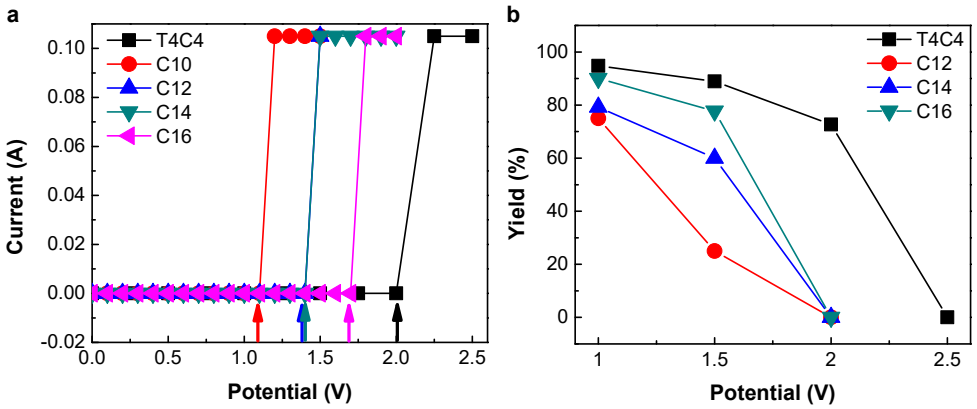

Figure 2.11 | Characterization on the electrical stability of **T4C4** and **C*n*** SAMs. **a**, Representative I/V plots show the breakdown voltages of Ag^{TS}/SAM//EGaIn junctions comprising **T4C4**, **C10**, **C12**, **C14** and **C16**. **b**, Yield of non-shorting junctions as a function of potential window.

percent-yield of non-shorting junctions scanned from ±1 V, ±1.5 V, ±2 V and ±2.5 V. All SAMs shorted 100 % of the time at ±2.5 V, but only 20 % of junctions comprising **T4C4** shorted at ±2 V, whereas 100 % of junctions comprising **C12**, **C14** and **C16** shorted. At ±1 V and ±1.5 V there is a clear trend of increasing percentage of shorts: **C12** > **C14** > **C16** > **T4C4**. This trend supports the hypothesis that the primary mode of failure of these Ag^{TS}/SAM//EGaIn junctions is mechanical failure due to electrostatic pressure from the applied bias; the mechanical robustness of SAMs of alkanethiolates scales with chain-length, but **T4C4** is considerably more robust than a SAM of alkanethiolates of any number of carbons up to at least **C16**.

2.3. CONCLUSIONS

Technological applications of molecular electronics in the medium-term will almost certainly utilize SAMs; they simplify fabrication and large-area junctions, in particular, can already be incorporated into integrated circuits and wafer-scale manufacturing processes. The usefulness of molecular tunneling junctions derives from the nonlinear dependence of I/V characteristics on the conformation and electronic structure of the molecules. However, the I/V properties of bottom-up junctions comprising SAMs are affected by mechanical force. For SAMs of alkanethiolates, mechanical forces disturb the packing of the SAM, causing tilt angles to increase. We have shown that the electronic structure of π-conjugated molecules (*i.e.*, the electrostatics of the junction) is also directly affected by mechanical force. Thus, it is important to develop an understanding of this relationship and relate it to molecular structure such that the mechanical properties of a SAM and how a tunneling junction responds to forces can be tailored synthetically both to increase the robustness and stability of junctions and to develop devices that respond to mechanical inputs.

We have shown that SAMs of a σ-π molecule designed to maximize intermolecular

interactions, **T4C4**, are significantly more mechanically robust than SAMs of alkanethiolates. SAMs of **T4C4** undergo less deformation as a function of force load by AFM and Young's modulus is approximately five times higher. At relatively low force loads, tunneling junctions comprising SAMs of **T4C4** show no changes in conductance or values of V_{trans}; SAMs of **C10** show significant changes. At higher force loads than SAMs of **C10** are capable of withstanding, junctions comprising **T4C4** begin to show differences. Our results demonstrate that it is possible to design molecules that maximize mechanical properties in large-area tunneling junctions comprising SAMs.

2.4. EXPERIMENTAL

2.4.1. PREPARATION OF SELF-ASSEMBLED MONOLAYERS

The formation of SAMs follows the reported methods.[33] The Ag and Au substrates were prepared by Template Stripping (TS) described in details elsewhere.[29] 200 nm of Ag (99.99%) and 100 nm of Au (99.99 %) were deposited by thermal deposition at 10^{-7} mbar onto a 3" Silicon wafer (without adhesion layer). Glass substrates (1 cm × 1 cm) were glued onto deposited metal by using UV-curable Optical Adhesive (Norland 61) with 300s exposure of UV. All samples were made by incubation of freshly cleaved silver and gold substrates into either 3 mM solution of the corresponding n-alkanethiols (n = 10, 12, 14, 16) in ethanol or 0.5 mM solution of **T4C4** in toluene at room temperature and kept inside a nitrogen flow box (in which the O_2 was below 3 % and the humidity was below 10 %) for 3 hr. Then the substrates of alkanethiols and **T4C4** were rinsed by ethanol and toluene respectively and dried gently by N_2. Prior to forming the SAMs, the solution was degassed by bubbling N_2 for at least 20 minutes and all solution were kept under N_2 atmosphere to prevent oxidation of thiol and Ag substrates.

2.4.2. CHARACTERIZATION OF ELECTRICAL PROPERTIES

CP-AFM I/V measurements were performed on a Bruker AFM Multimode MMAFM-2 equipped with a PeakForce TUNA application module (Bruker). The SAMs were contacted with an Au-coated silicon nitride tip with a nominal radius of 30 nm (NPG-10, Bruker, tip A: resonant frequency: 65 kHz, spring constant: 0.35 N/m; tip B: resonant frequency: 23 kHz, spring constant: 0.12 N/m; tip D: resonant frequency: 18 kHz, spring constant: 0.06 N/m. Tip A was chosen in this work) in TUNA mode. The AFM tip was grounded and for all force loads, **T4C4** on Au^{TS} were biased from -1 V to 1 V and from 1 V to -1 V while **C10** on were biased from -1.5 V to 1.5 V and from 1.5 V to -1.5 V on Au^{TS} to record the I/V curves: a max of 10 trace/re-trace cycles per junction were performed and the top electrode was removed from SAMs between junctions. Between different samples a new tip was used. It is difficult to determine V_{trans} for an individual I/V trace due to the inherent noise in the raw data. The peaks of Gaussian fits to the histograms of I for each value of V at different force loads obtained by CP-AFM were plotted and transformed into axes of $ln(IV^{-2})$ versus V^{-1}. The position of the V_{trans} was determined by manually picking the center of the dips in the plots. The total number of I/V traces recorded by CP-AFM is summarized in Table 2.4.

Table 2.4 | Summary of number of I/V traces recorded by CP-AFM in this work.

	Force(nN)	Traces		Force(nN)	Traces
T4C4(Au)	**1.4**	202	**C10(Au)**	**1.4**	30
	3.5	198		**5**	30
	5	200		**10**	30
	10	179			
	25	156			
	50	200			
	75	198			
	100	198			
T4C4(Ag)	**2**	52	**C10(Ag)**	**1.4**	21
	25	51		**5**	10
	50	52		**10**	20
	75	54		**25**	21
	100	51		**50**	20
	125	47	**C12(Ag)**	**2**	35
	150	81		**25**	48
				50	48
				75	49
				100	74
				125	37
				150	48

EGaIn The measurements with EGaIn, as well as the sample preparation and handling, were performed in the nitrogen flow box in which O_2 was maintained below 3 % and the humidity was kept below 10 %. At least two samples were examined for each molecule. The potential windows include: 1) 0 V→ 1 V→ −1 V→ 0 V, steps of 0.05 V; 2) 0 V→ 1.5 V→ −1.5 V→ 0 V, steps of 0.1 V; 3) 0 V→ 2 V→ −2 V→ 0 V, steps of 0.1 V; 4) 0 V→ 2.5 V→ −2.5 V→ 0 V, steps of 0.25 V. 20 trace/re-trace cycles were measured for each junction and shorts occur during the cycles is counted for the failure of junction.

2.4.3. PEAKFORCE QNM MEASUREMENTS

The measurements of Young's modulus of the SAMs were performed on a Bruker Multimode MMAFM-2 in PeakForce QNM® mode. The tips used in the measurements were ScanAsyst-Air from Bruker (resonant frequency: 70kHz, spring constant: 0.4N/m, tip radius: 2nm). Deflection sensitivity was calibrated by measuring 5 force curves on fused silica sample provided by Bruker and taking the average of the results. Spring constant was calibrated by thermal tune before and after the measurements. Tip radius was calibrated before and after the measurements using scanning electron microscope (SEM). Deformation under each force load was measured from 5 spots of the sample and averaged. Young's modulus was calculated by DMT model from the averaged deformation of each force load.

2.4.4. I/V DATA PROCESSING

Data were acquired as described above and then parsed in a "hands-off" manner using Scientific Python to produce histograms of I for each value of V and the associated Gaussian fits (using a least-squares fitting routine).

The I/V curve of **T4C4** in all range of force loads (from 1.4 nN to 100 nN) is shown in Fig. 2.4a and current of **T4C4** and **C10** at 1.0 V or -1.0 V versus force load is shown in Fig. 2.4b.

Figs 2.5 and 2.6 shows the results of I/V characterization on Ag^{TS} substrate. **C12** on Ag^{TS}, the samples were biased from -2 V to 2 V and from 2 V to -2 V and **C10**, **T4C4** on Ag^{TS}, the samples were biased from -1.5 V to 1.5 V and from 1.5 V to -1.5 V.

2.4.5. ESTIMATION OF CONTACT AREA

The measurements of Young's modulus were performed on a Bruker AFM Multimode MMAFM-2. The SAMs were contacted with a silicon nitride tip with a nominal radius of 2 nm (ScanAsyst-Air, Bruker, resonant frequency 70 kHz, spring constant: 0.4N/m) in PeakForce QNM mode. The deflection sensitivity, spring constant of the cantilever and tip radius were calibrated both before and after the measurement. Samples were scanned in ScanAsyst Mode for selecting a region where dust particles or other contaminants were not present. Deformation of the sample were measured under a force load ranging from 0.13 nN to 19.62 nN over 5 positions and later used to calculate Young's modulus from DMT model in Nanoscope Analysis (Bruker). The contact area of Au tip is calculated based on reported work[19], in which the radius of the contact area between the Au AFM tip and **C10** SAM changes linearly with the force as shown in Eq. 2.1.

$$A = 1.70F + 100.8 \tag{2.1}$$

in which A is the contact area (nm^2) between the AFM tip and the SAM, F is the force load. The pressure is then calculated from load force divided by contact area.

In the case of Si_3N_4 tip, the part where the tip is in contact with the SAM is considered as a spherical cap. The deformation h is the height of the cap and the radius of the tip is the radius of the sphere R. We simplified the contact area between the AFM tip and the SAM as the projection of the spherical cap on the plane of the SAM. Then the contact area can be calculated from

$$A = \pi[R^2 - (R-h)^2] \tag{2.2}$$

Similar to the case of Au tip, the pressure is then calculated from load force divided by contact area.

Table 2.5 | Summary of different Load Forces, Contact Areas and Pressures by AFM Tip in this work.

	Force Load (nN)	**Contact Area (nm^2)**	**Applied Pressure (MPa)**
Au tip	**1.4**	103.17	163.12
	3.5	106.74	177.35
	5	109.28	186.94
	10	117.77	215.93
	25	143.23	282.28
	50	185.65	352.43
	75	228.08	396.49
	100	270.51	426.72
Si_3N_4 tip	**0.13**	2.72	48.11
	0.65	4.52	144.64
	1.31	7.01	186.99
	1.96	7.25	270.22
	2.62	8.55	306.41
	3.27	9.29	351.87
	3.93	10.50	374.29
	4.58	10.75	426.19
	5.23	11.50	454.64
	5.89	11.43	515.33
	6.54	11.39	574.11

2.4.6. EGAIN STABILITY TEST

The statistics of the stability test on EGaIn junctions are summarized in Table 2.6. Each junction was scanned with 20 trace/re-trace cycles. At least two samples were examined for each molecule. Fig. 2.12 shows the plots of J/V curves for Ag^{TS}/ SAMs//EGaIn junctions comprising **T4C4**, **C12**, **C14**, **C16**.

Table 2.6 | Yields of EGaIn junctions on Ag^{TS} at different voltages.

	Voltage	Total	Working	Short	Yield
T4C4	**1.0V**	58	55	3	94.83%
	1.5V	9	8	1	88.9%
	2.0V	11	8	3	72.7%
	2.5V	10	0	10	0%
C12	**1.0V**	36	27	9	75%
	1.5V	8	2	6	25%
	2.0V	8	0	8	0%
C14	**1.0V**	24	19	5	79.2%
	1.5V	20	12	8	60%
	2.0V	10	0	10	0%
C16	**1.0V**	10	9	1	90%
	1.5V	9	7	2	77.7%
	2.0V	10	0	10	0%

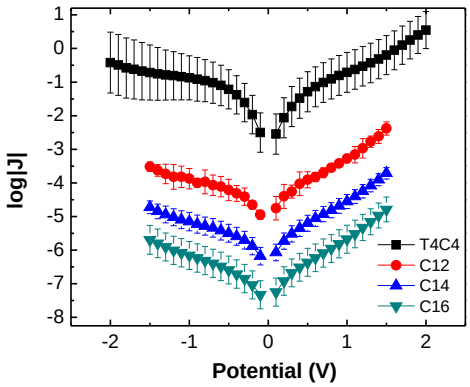

Figure 2.12 | Plots of $\log|J|$-V curves (the unit of J is $\log|J(\mathrm{A\,cm^{-2}})|$) in Ag^{TS}/**T4C4**//EGaIn junctions: black square for **T4C4**, red circle for **C12**, blue up-triangle for **C14**, dark cyan down-triangle for **C16**. Each data point is the mean of Gaussian fit to the histogram of $\log|J|$for that value of V and the error bars are the 95 % confidence intervals.

REFERENCES

[1] R. F. Service, *The brain chip,* Science **345**, 614 (2014).

[2] D. Xiang, X. Wang, C. Jia, T. Lee, and X. Guo, *Molecular-scale electronics: from concept to function,* Chem. Rev. **116**, 4318 (2016).

[3] G. Wang, Y. Kim, S. I. Na, Y. H. Kahng, J. Ku, S. Park, Y. H. Jang, D. Y. Kim, and T. Lee, *Investigation of the transition voltage spectra of molecular junctions considering frontier molecular orbitals and the asymmetric coupling effect,* J. Phys. Chem. C **115**, 17979 (2011).

[4] X. D. Cui, A. Primak, X. Zarate, J. Tomfohr, O. F. Sankey, A. L. Moore, T. A. Moore, D. Gust, G. Harris, and S. M. Lindsay, *Reproducible measurement of single-molecule conductivity,* Science **294**, 571 (2001).

[5] N. J. Tao, *Electron transport in molecular junctions,* Nat. Nanotechnol. **1**, 173 (2006).

[6] H. B. Akkerman, P. W. M. Blom, D. M. de Leeuw, and B. de Boer, *Towards molecular electronics with large-area molecular junctions,* Nature **441**, 69 (2006).

[7] G. Wang, Y. Kim, M. Choe, T. W. Kim, and T. Lee, *A new approach for molecular electronic junctions with a multilayer graphene electrode,* Adv. Mater. **23**, 755 (2011).

[8] Y. Zhang, Z. Zhao, D. Fracasso, and R. C. Chiechi, *Bottom-up molecular tunneling junctions formed by self-assembly,* Isr. J. Chem. **54**, 513 (2014).

[9] P. A. van Hal, E. C. P. Smits, T. O. M. C. T. Geuns, H. B. Akkerman, B. C. D. E. Brito, S. Perissinotto, G. Lanzani, A. J. Kronemeijer, M. E. Cornil, P. W. M. Blom, B. de Boer, and D. M. de Leeuw, *Upscaling , integration and electrical characterization of molecular junctions,* Nat. Nanotechnol. **3**, 749 (2008).

[10] A. Wan, C. S. S. Sangeeth, L. Wang, L. Yuan, L. Jiang, and C. A. Nijhuis, *Arrays of high quality SAM-based junctions and their application in molecular diode based logic,* Nanoscale , 19547 (2015).

[11] A. Kovalchuk, T. Abu-Husein, D. Fracasso, D. A. Egger, E. Zojer, M. Zharnikov, A. Terfort, and R. C. Chiechi, *Transition voltages respond to synthetic reorientation of embedded dipoles in self-assembled monolayers,* Chem. Sci. **7**, 781 (2016).

[12] M. Carlotti, A. Kovalchuk, T. Wächter, X. Qiu, M. Zharnikov, and R. C. Chiechi, *Conformation-driven quantum interference effects mediated by through-space conjugation in self-assembled monolayers,* Nat. Commun. **7**, 1 (2016).

[13] N. Nerngchamnong, L. Yuan, D. C. Qi, J. Li, D. Thompson, and C. A. Nijhuis, *The role of van der Waals forces in the performance of molecular diodes,* Nat. Nanotechnol. **8**, 113 (2013).

[14] A. Kovalchuk, D. A. Egger, T. Abu-Husein, E. Zojer, A. Terfort, and R. C. Chiechi, *Dipole-induced asymmetric conduction in tunneling junctions comprising self-assembled monolayers,* RSC Adv. **6**, 69479 (2016).

[15] L. Venkataraman, J. E. Klare, C. Nuckolls, M. S. Hybertsen, and M. L. Steigerwald, *Dependence of single-molecule junction conductance on molecular conformation,* Nature **442**, 904 (2006).

[16] D. J. Wold and C. D. Frisbie, *Fabrication and characterization of metal-molecule-metal junctions by conducting probe atomic force microscopy,* J. Am. Chem. Soc. **123**, 5549 (2001).

[17] H. Song, H. Lee, and T. Lee, *Intermolecular chain-to-chain tunneling in metal-alkanethiol-metal junctions,* J. Am. Chem. Soc. **129**, 3806 (2007).

[18] Y. Qi, I. Ratera, J. Y. Park, P. D. Ashby, S. Y. Quek, J. B. Neaton, and M. Salmeron, *Mechanical and charge transport properties of alkanethiol self-assembled monolayers on a Au(111) surface: The role of molecular tilt,* Langmuir **24**, 2219 (2008).

[19] G. Wang, T. W. Kim, G. Jo, and T. Lee, *Enhancement of field emission transport by molecular tilt configuration in metal-molecule-metal junctions,* J. Am. Chem. Soc. **131**, 5980 (2009).

[20] K. Smaali, S. Desbief, G. Foti, T. Frederiksen, D. Sanchez-Portal, A. Arnau, J. P. Nys, P. Leclère, D. Vuillaume, and N. Clément, *On the mechanical and electronic properties of thiolated gold nanocrystals,* Nanoscale **7**, 1809 (2015).

[21] J. M. Beebe, B. Kim, J. W. Gadzuk, C. D. Frisbie, and J. G. Kushmerick, *Transition from direct tunneling to field emission in metal-molecule-metal junctions,* Phys. Rev. Lett. **97**, 1 (2006).

[22] R. C. Chiechi, E. A. Weiss, M. D. Dickey, and G. M. Whitesides, *Eutectic gallium–indium (EGaIn): a moldable liquid metal for electrical characterization of self-assembled monolayers,* Angew. Chem. Int. Ed. **47**, 142 (2008).

[23] Y. Zhang, X. Qiu, P. Gordiichuk, S. Soni, T. L. Krijger, A. Herrmann, and R. C. Chiechi, *Mechanically and Electrically Robust Self-Assembled Monolayers for Large-Area Tunneling Junctions,* J. Phys. Chem. C **121**, 14920 (2017).

[24] B. De Boer, H. Meng, D. F. Perepichka, J. Zheng, M. M. Frank, Y. J. Chabal, and Z. Bao, *Synthesis and characterization of conjugated mono- and dithiol oligomers and characterization of their self-assembled monolayers,* Langmuir **19**, 4272 (2003).

[25] B. Liedberg, Z. Yang, I. Engquist, M. Wirde, U. Gelius, G. Götz, P. Bäuerle, R. M. Rummel, C. Ziegler, and W. Göpel, *Self-assembly of α-functionalized terthiophenes on gold,* J. Phys. Chem. B **101**, 5951 (1997).

[26] H. S. Kato, Y. Murakami, Y. Kiriyama, R. Saitoh, T. Ueba, T. Yamada, Y. Ie, Y. Aso, and T. Munakata, *Decay of the exciton in quaterthiophene terminated alkanethiolate self assembled monolayers on Au(111),* J. Phys. Chem. C **119**, 7400 (2015).

[27] J. M. Beebe, V. B. Engelkes, L. L. Miller, and C. D. Frisbie, *Contact Resistance in Metal - Molecule - Metal Junctions Based on Aliphatic SAMs : Effects of Surface Linker and Metal Work Function,* J. Am. Chem. Soc. **124**, 11268 (2002).

[28] J. M. Beebe, B. S. Kim, C. D. Frisbei, and J. G. Kushmerick, *Measuring relative barrier heights in molecular electronic junctions with transition voltage spectroscopy,* ACS Nano **2**, 827 (2008).

[29] E. A. Weiss, G. K. Kaufman, J. K. Kriebel, Z. Li, R. Schalek, and G. M. Whitesides, *Si/SiO2-templated formation of ultraflat metal surfaces on glass, polymer, and solder supports: Their use as substrates for self-assembled monolayers,* Langmuir **23**, 9686 (2007).

[30] E. A. Weiss, R. C. Chiechi, G. K. Kaufman, J. K. Kriebel, Z. Li, M. Duati, M. A. Rampi, and G. M. Whitesides, *Influence of defects on the electrical characteristics of mercury-drop junctions: Self-assembled monolayers of n-alkanethiolates on rough and smooth silver,* J. Am. Chem. Soc. **129**, 4336 (2007).

[31] S. H. Choi, C. Risko, M. Carmen Ruiz Delgado, B. Kim, J. L. Brédas, and C. Daniel Frisbie, *Transition from Tunneling to Hopping Transport in Long, Conjugated Oligo-imine Wires Connected to Metals,* J. Am. Chem. Soc. **132**, 4358 (2010).

[32] D. Xiang, Y. Zhang, F. Pyatkov, A. Offenhäusser, and D. Mayer, *Gap size dependent transition from direct tunneling to field emission in single molecule junctions,* Chem. Commun. **47**, 4760 (2011).

[33] L. Jiang, C. S. Sangeeth, and C. A. Nijhuis, *The Origin of the Odd-Even Effect in the Tunneling Rates across EGaIn Junctions with Self-Assembled Monolayers (SAMs) of n-Alkanethiolates,* J. Am. Chem. Soc. **137**, 10659 (2015).

[34] F. C. Simeone, H. J. Yoon, M. M. Thuo, J. R. Barber, B. Smith, and G. M. Whitesides, *Defining the value of injection current and effective electrical contact area for egain-based molecular tunneling junctions,* J. Am. Chem. Soc. **135**, 18131 (2013).

[35] M. Carlotti, M. Degen, Y. Zhang, and R. C. Chiechi, *Pronounced environmental effects on injection currents in EGaIn tunneling junctions comprising self-assembled monolayers,* J. Phys. Chem. C **120**, 20437 (2016).

[36] M. E. Dokukin and I. Sokolov, *Quantitative mapping of the elastic modulus of soft materials with HarmoniX and PeakForce QNM AFM modes,* Langmuir **28**, 16060 (2012).

[37] B. Derjaguin, V. Muller, and Y. Toporov, *Effect of contact deformation on the adhesion of particles.* J. Colloid Interface Sci. **52**, 105 (1975).

[38] F. W. Delrio, C. Jaye, D. A. Fischer, and R. F. Cook, *Elastic and adhesive properties of alkanethiol self-assembled monolayers on gold,* Appl. Phys. Lett. , 131909 (2009).

[39] G. Ricœur, S. Lenfant, D. Guérin, and D. Vuillaume, *Molecule/electrode interface energetics in molecular junction: A "transition voltage spectroscopy" study,* J. Phys. Chem. C **116**, 20722 (2012).

[40] Z. Xie, I. Bâldea, C. E. Smith, Y. Wu, and C. D. Frisbie, *Experimental and Theoretical Analysis of Nanotransport in Oligophenylene Dithiol Junctions as a Function of Molecular Length and Contact Work Function,* ACS Nano **9**, 8022 (2015).

[41] B. Kim, S. H. Choi, X. Y. Zhu, and C. D. Frisbie, *Molecular tunnel junctions based on π-conjugated oligoacene thiols and dithiols between Ag, Au, and Pt contacts: Effect of surface linking group and metal work function,* J. Am. Chem. Soc. **133**, 19864 (2011).

[42] Z. Xie, I. Bâldea, and C. D. Frisbie, *Why one can expect large rectification in molecular junctions based on alkane monothiols and why rectification is so modest,* Chem. Sci. **9**, 4456 (2018).

[43] Z. Xie, I. Bâldea, G. Haugstad, and C. Daniel Frisbie, *Mechanical deformation distinguishes tunneling pathways in molecular junctions,* J. Am. Chem. Soc. **141**, 497 (2019).

[44] K. Slowinski, R. V. Chamberlain, C. J. Miller, and M. Majda, *Through-bond and chain-to-chain coupling. Two pathways in electron tunneling through liquid alkanethiol monolayers on mercury electrodes,* J. Am. Chem. Soc. **119**, 11910 (1997).

[45] J. C. Love, L. A. Estroff, J. K. Kriebel, R. G. Nuzzo, and G. M. Whitesides, *Self-Assembled Monolayers of Thiolates on Metals as a Form of Nanotechnology,* Chem. Rev. **105**, 1103 (2005).

[46] L. Jiang, C. S. Sangeeth, A. Wan, A. Vilan, and C. A. Nijhuis, *Defect scaling with contact area in EGaIn-based junctions: impact on quality, Joule heating, and apparent injection current,* J. Phys. Chem. C **119**, 960 (2015).

[47] L. Jiang, C. S. Sangeeth, L. Yuan, D. Thompson, and C. A. Nijhuis, *One-nanometer thin monolayers remove the deleterious effect of substrate defects in molecular tunnel junctions,* Nano Lett. **15**, 6643 (2015).

[48] K. Slowinski and M. Majda, *Mercury-mercury tunneling junctions - Part II. Structure and stability of symmetric alkanethiolate bilayers and their effect on the rate of electron tunneling,* J. Electroanal. Chem. **491**, 139 (2000).

[49] C. A. Nijhuis, W. F. Reus, J. R. Barber, M. D. Dickey, and G. M. Whitesides, *Charge transport and rectification in arrays of SAM-based tunneling junctions,* Nano Lett. **10**, 3611 (2010).

[50] W. Haiss, S. Martín, E. Leary, H. Van Zalinge, S. J. Higgins, L. Bouffier, and R. J. Nichols, *Impact of junction formation method and surface roughness on single molecule conductance,* J. Phys. Chem. C **113**, 5823 (2009).

[51] J. Chen, M. Kim, S. Gathiaka, S. J. Cho, S. Kundu, H. J. Yoon, and M. M. Thuo, *Understanding Keesom interactions in monolayer-based large-area tunneling junctions,* J. Phys. Chem. Lett. **9**, 5078 (2018).

[52] G. Philipp, C. Müller-Schwanneke, M. Burghard, S. Roth, and K. V. Klitzing, *Gold cluster formation at the interface of a gold/Langmuir-Blodgett film/gold microsandwich resulting in Coulomb charging phenomena,* J. Appl. Phys. **85**, 3374 (1999).

[53] N. B. Zhitenev, A. Erbe, Z. Bao, W. Jiang, and E. Garfunkel, *Molecular nano-junctions formed with different metallic electrodes,* Nanotechnology **16**, 495 (2005).

[54] O. Seitz, A. Vilan, H. Cohen, J. Hwang, M. Haeming, A. Schoell, E. Umbach, A. Kahn, and D. Cahen, *Doping molecular monolayers: Effects on electrical transport through alkyl chains on silicon,* Adv. Funct. Mater. **18**, 2102 (2008).

[55] C. A. Nijhuis, W. F. Reus, A. C. Siegel, and G. M. Whitesides, *A molecular half-wave rectifier,* J. Am. Chem. Soc. **133**, 15397 (2011).

[56] C. A. Nijhuis, W. F. Reus, and G. M. Whitesides, *Molecular rectification in metal-SAM-metal oxide-metal junctions,* J. Am. Chem. Soc. **131**, 17814 (2009).

[57] L. Yuan, R. Breuer, L. Jiang, M. Schmittel, and C. A. Nijhuis, *A Molecular Diode with a Statistically Robust Rectification Ratio of Three Orders of Magnitude,* Nano Lett. **15**, 5506 (2015).

[58] H. J. Yoon, K. C. Liao, M. R. Lockett, S. W. Kwok, M. Baghbanzadeh, and G. M. Whitesides, *Rectification in tunneling junctions: 2,2'-bipyridyl-terminated n -alkanethiolates,* J. Am. Chem. Soc. **136**, 17155 (2014).

[59] G. D. Kong, M. Kim, S. J. Cho, and H. J. Yoon, *Gradients of Rectification: Tuning Molecular Electronic Devices by the Controlled Use of Different-Sized Diluents in Heterogeneous Self-Assembled Monolayers,* Angew. Chem. Int. Ed. **55**, 10307 (2016).

[60] L. Qiu, Y. Zhang, T. L. Krijger, X. Qiu, P. v. t. Hof, J. C. Hummelen, and R. C. Chiechi, *Rectification of current responds to incorporation of fullerenes into mixed-monolayers of alkanethiolates in tunneling junctions,* Chem. Sci. **8**, 2365 (2017).